



As. Zh. Khurshudyan 

# A mesoscopic model for particle-reinforced composites

*To the memory of Prof. Eduard Kh. Grigoryan (1938–2016) is dedicated.*

Received: 6 January 2019 / Accepted: 5 July 2019 / Published online: 18 July 2019  
© Springer-Verlag GmbH Germany, part of Springer Nature 2019

**Abstract** The effective or homogenized properties of particle-reinforced composites, which characterize their macroscopic behavior, do not contain any information about location of individual particles, thus limiting the possibilities of studying the influence of specific distributions of particles on the composites behavior. As a consequence, determination of optimal (in an appropriate sense) configuration of reinforcing particles is also restricted. This problem is addressed in this paper by deriving a mesoscopic model for particle-reinforced composites from the microscopic model of a continuum reinforced by a set of spherical inclusions. As a result, at the mesoscale, the composite is represented as a continuum with point inhomogeneities. At this, characteristics and location of each individual particle enter into the material properties of the composite explicitly. Theoretical derivations are supported by a numerical example of a Mindlin–Reissner thick plate reinforced over its mid-plane by a set of inclusions and subjected to a vertical load distributed over its upper surface.

**Keywords** Particle-reinforced materials · Mesoscopic model · Theory of distributions · Mindlin–Reissner plate theory

## 1 Introduction

Composite materials have widespread applications in such areas as civil and aerospace engineering, machinery, robotics, etc. In order to widen the range of their practical use, composite materials with improved structures are designed continuously. These improvements, however, require consistent theoretical developments based on mathematical modeling and since composite materials generally exhibit different features at different (length) scales, multiscale modeling turns out to be the basic tool for that purpose [1, 2]. The typical procedure of multiscale modeling of composites can be summarized as follows. The microstructure of the composite is accurately modeled taking into account all its microscale features. Then, the corresponding macroscopic model is derived by using diverse methods of homogenization [3], such as averaging [4],  $G$ -,  $H$ - or  $\Gamma$ -convergence [5]. As a result, the behavior of microscopically inhomogeneous composites at the macroscale is described by equations of fully homogeneous structures, the homogenized (more often referred to as effective) material properties

---

Communicated by Andreas Öchsner.

As. Zh. Khurshudyan (✉)  
Department on Dynamics of Deformable Systems and Coupled Fields, Institute of Mechanics, National Academy of Sciences of Armenia, Yerevan, Armenia  
E-mail: khurshudyan@sju.edu.cn; khurshudyan@mechins.sci.am

As. Zh. Khurshudyan  
Institute of Natural Sciences, Shanghai Jiao Tong University, Shanghai, China

of which are uniquely derived from the corresponding microscopic quantities. There exist multiple well-developed methods for exact and approximate evaluation of homogenized properties of composites depending on different features of microscale inhomogeneities such as shape, individual properties, distributions, etc. [6,7]. Nonetheless, the location of each individual inhomogeneity is not always made explicit in the expressions of effective properties. Taking into account the contemporary powerful means of material processing at the microlevel, such as microadditive manufacturing [8], this becomes a serious limitation of possibilities for optimal design of composites by means of appropriate choice of their microstructure. The missing link in this chain which will allow to consider microstructure optimization of composites is the mesoscopic model [9].

The purpose of this paper is to fill this gap in the case of particle-reinforced composites by deriving their mesoscopic model, the material properties of which explicitly depend on material properties and spatial location of each individual particle. As other types of reinforced composites, these are regarded as microscopically inhomogeneous reinforced by inclusions of different shapes such as ellipsoidal or spherical [10]. Even though there exist several efficient models for identification and estimation of effective (homogenized) properties of multi-phase particle-reinforced composites at the macroscale [11–19], there is nothing for their material properties at the mesoscale where, according to their natural treatment, particles can be regarded as point inhomogeneities. It is worth a separate mentioning contributions [20,21], where closed-form formulas for effective properties of composites with spherical nanoinhomogeneities are derived using the complete Gurtin–Murdoch model for the composite and reinforcing particles interface.

The microscopic model considered in this paper mainly lays on the following four assumptions concerning the inclusions and bulk material: (i) both bulk and inclusions are free of any voids or defects, (ii) inclusions are embedded into the bulk firmly and perfectly, i.e., there are no imperfections at the common interface, (iii) all inclusions are (geometrically and physically) identical balls of finite diameter, (iv) inclusions do not interact with each other during the deformation. The first two assumptions imply that the elastic properties of the composite are piecewise constant functions and, therefore, they can be represented as functions of local coordinates in terms of the indicator function of the bulk and inclusions. Note that the assumption (ii) has been relaxed in a series of recent papers [16,22,23], where formulas for effective material characteristics of particle-reinforced composites are derived using the deterministic and stochastic homogenization under the assumption that there may exist defects on the interface of the bulk and particles. The assumption (iv) can be relaxed using the model developed in [24].

Under these assumptions, accepting also linear constitutive law and linear kinematic relations, Navier–Lamé equations are derived for microscopic displacements of the composite. Letting the diameter of inclusions decrease to 0, the corresponding equations are derived for the mesoscopic displacements of the composite and convergence between the microscopic and mesoscopic displacements is established using the reduced basis Bubnov–Galerkin procedure. The mesoscopic density and Young’s modulus are expressed in terms of Dirac  $\delta$  distribution concentrated at centers of the reinforcing inclusions corresponding to a continuum with point inhomogeneities. As a particular case, a Mindlin–Reissner plate reinforced with a set of identical inclusions over its mid-plane and subjected to a normal load distributed over its upper surface is considered. Numerical analysis of the microscopic model for a decreasing sequence of the diameter and the mesomodel (diameter tends to 0) reveals convergence of moment and shear resultants of the plate mid-plane as well.

## 2 Preliminaries

### 2.1 Notations

By a three-dimensional body  $\mathbf{B}$ , a continuum material occupying a bounded open domain  $\Omega \subset \mathbb{R}^3$  with a sufficiently regular boundary  $\partial\Omega$  is implied. As usual, material points are denoted by  $\mathbf{x} = (x_1, x_2, x_3)$ .

A set  $\mathbf{b}^d = \bigcup_{n=1}^N \mathbf{b}_n^d \subset \Omega$  of identical, homogeneous spherical inclusions  $\mathbf{b}_n^d = \{\mathbf{x} \in \Omega, 4|\mathbf{x} - \mathbf{x}_{0n}|^2 \leq d^2\}$

of arbitrary *finite* number  $N \in \mathbb{N}$  is considered with constant volume fraction denoted by  $\phi_{\text{incl}}$ . The bulk counterpart of  $\mathbf{B}$  is denoted by  $\mathbf{B}_b^d = \mathbf{B} \setminus \mathbf{b}^d$  which is supposed to be homogeneous. Assume that both  $\mathbf{B}_b^d$  and  $\mathbf{b}_n^d$  are filled with material continuously, i.e., they are free of any defects. The inclusions do not overlap in both undeformed and deformed configurations, i.e.,  $\mathbf{b}_n^d \cap \mathbf{b}_m^d = \emptyset$  for  $n \neq m$ , and inclusions do not intersect with the boundary of  $\mathbf{B}$ , i.e.,  $\mathbf{b}^d \cap \partial\Omega = \emptyset$ .

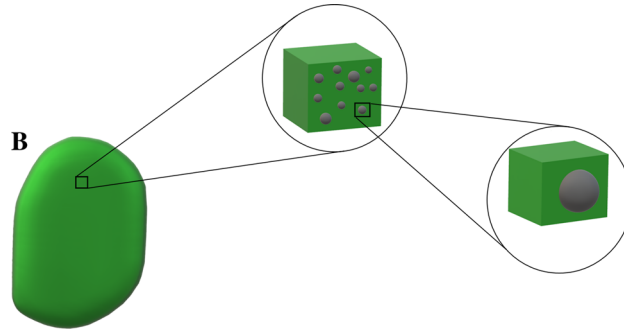


**Fig. 1** Schematic representation of a continuum with firmly embedded spherical inclusions

Here,  $d$  is the diameter of inclusions,  $\mathbf{x}_{0n}$  is the center of the  $n$ th inclusion in a Cartesian coordinate system attached to  $\mathbf{B}$ ,  $|\cdot|$  denotes the Euclidean norm in  $\mathbb{R}^3$ . The set of inclusions centers is denoted by  $\mathbf{b}^0 = \bigcup_{n=1}^N \{\mathbf{x}_{0n}\}$ . It is also assumed that  $d$  is small compared to the smallest characteristic measure of  $\mathbf{B}$ . For instance, if  $\mathbf{B}$  is a beam, plate or shell of thickness  $h$ , then  $d \ll h$ . See, Fig. 1.

2.2 Some definitions

In order to characterize the material properties of  $\mathbf{B}$ , the following distributions are introduced defined with the aim of compactly supported test functions  $\varphi \in C^\infty(\mathbf{b}_n^d)$ ,  $\text{supp}(\varphi) \subseteq \mathbf{b}_n^d$ , where  $\text{supp}(\varphi) = \overline{\{\mathbf{x} \in \mathbb{R}^3, \varphi \neq 0\}}$  is the support of  $\varphi$ .

1. Distribution generated by the characteristic (indicator) function  $\chi_{\mathbf{b}_n^d}$ :

$$(\chi_{\mathbf{b}_n^d}, \varphi) = \int_{\mathbb{R}^3} \chi_{\mathbf{b}_n^d}(\mathbf{x}) \varphi(\mathbf{x}) \, d\mathbf{x} = \int_{\mathbf{b}_n^d} \varphi(\mathbf{x}) \, d\mathbf{x}.$$

2. Distribution generated by the Heaviside  $\theta$  function

$$(\theta, \varphi) = \int_{(\mathbb{R}^+)^3} \varphi(\mathbf{x}) \, d\mathbf{x},$$

3. Distribution generated by the Dirac  $\delta$  function

$$(\delta, \varphi) = \varphi(\mathbf{0}). \tag{1}$$

The connection between these distributions is as follows:

$$\chi_{\mathbf{b}_n^d}(\mathbf{x}) = \theta\left(\frac{1}{4}d^2 - |\mathbf{x} - \mathbf{x}_{0n}|^2\right), \tag{2}$$

and

$$\delta(\mathbf{x}) = \theta'(\mathbf{x}).$$

The derivative is understood in the sense of distributions.

**Definition 1** The sequence of functions  $f^d$  is said to converge to distribution  $f^0$  as  $d \rightarrow 0$  in the sense of distributions, if

$$(f^d, \varphi) \rightarrow (f^0, \varphi) \text{ as } d \rightarrow 0,$$

for every compactly supported test function  $\varphi$ .

Kronecker's symbol is denoted by  $\delta_i^j$ :

$$\delta_i^j = \begin{cases} 1, & i = j, \\ 0, & i \neq j. \end{cases}$$

### 2.3 Volume, mass, density and Young's modulus

Assume that inclusions are embedded into the bulk material firmly, i.e., there are no any defects or voids at the common interface of  $\mathbf{B}_b^d$  and any of  $\mathbf{b}_n^d$ . Denote by  $V_{\mathbf{B}_b^d}$  and  $V_{\mathbf{b}_n^d}$  the volume of the bulk and a typical inclusion, respectively. Then, the volume of  $\mathbf{B}$  would be

$$V_{\mathbf{B}} = V_{\mathbf{B}_b^d} + \sum_{n=1}^N V_{\mathbf{b}_n^d} = V_{\mathbf{B}_b^d} + N \frac{1}{6} \pi d^3 \quad (3)$$

Denote by  $m_{\text{bulk}}$  and  $m_{\text{incl}}$  the mass of the bulk and a typical inclusion, respectively. Then, the mass of  $\mathbf{B}$  would be

$$m = m_{\text{bulk}} + N m_{\text{incl}}.$$

Furthermore, the density of  $\mathbf{B}$ , denoted by  $\rho^d$ , characterizing its microstructure can be represented as a function of  $\mathbf{x}$  as follows:

$$\rho^d(\mathbf{x}) = \frac{m_{\text{bulk}}}{V_{\mathbf{B}_b^d}} \chi_{\mathbf{B}_b^d}(\mathbf{x}) + \sum_{n=1}^N \frac{m_{\text{incl}}}{V_{\mathbf{b}_n^d}} \chi_{\mathbf{b}_n^d}(\mathbf{x}), \quad \mathbf{x} \in \mathbf{B}. \quad (4)$$

Similar to (4), Young's modulus of  $\mathbf{B}$  can be represented as a function of  $\mathbf{x}$  with the aid of  $\chi_{\mathbf{B}_b^d}$  and  $\chi_{\mathbf{b}_n^d}$ ,

$$E^d(\mathbf{x}) = E_{\text{bulk}} \chi_{\mathbf{B}_b^d}(\mathbf{x}) + E_{\text{incl}} \sum_{n=1}^N \chi_{\mathbf{b}_n^d}(\mathbf{x}), \quad \mathbf{x} \in \mathbf{B}, \quad (5)$$

where  $E_{\text{bulk}}$  and  $E_{\text{incl}}$  are the constant Young's moduli of the bulk material and inclusions, respectively.

### 2.4 Limit of the characteristic function in the sense of distributions

The aim is to establish a mesoscopic model of deformation for  $\mathbf{B}$  reinforced with spherical inclusions  $\mathbf{b}_n^d$  as  $d \rightarrow 0$ . In particular, it will allow to study the effects associated with the number, spatial distribution and individual material properties of reinforcing particles, unlike fully macroscopic models relying on homogenization and calculation of effective properties of composites [19]. To this aim, the following result is important.

**Lemma 1** *In the sense of distributions,*

$$\frac{1}{V_{\mathbf{b}_n^d}} \chi_{\mathbf{b}_n^d}(\mathbf{x}) \rightarrow \delta(\mathbf{x} - \mathbf{x}_{0n}) \quad \text{as } d \rightarrow 0. \quad (6)$$

*Proof* According to the definition, as  $d \rightarrow 0$ ,

$$\frac{1}{V_{\mathbf{b}_n^d}} (\chi_{\mathbf{b}_n^d}, \varphi) = \frac{1}{V_{\mathbf{b}_n^d}} \int_{\mathbf{b}_n^d} \varphi(\mathbf{x}) \, d\mathbf{x} \rightarrow \varphi(\mathbf{x}_{0n}).$$

On the other hand, according to the definition,

$$\varphi(\mathbf{x}_{0n}) = \int_{\mathbb{R}^3} \delta(\mathbf{x} - \mathbf{x}_{0n}) \varphi(\mathbf{x}) \, d\mathbf{x}.$$

This is equivalent to (6).

Note that (6) can also be proved with the aid of (2). Indeed, as  $d \rightarrow 0$ ,

$$\theta\left(\frac{1}{4}d^2 - |\mathbf{x} - \mathbf{x}_{0n}|^2\right) \rightarrow \theta(-|\mathbf{x} - \mathbf{x}_{0n}|^2),$$

which differs from zero only when  $\mathbf{x} = \mathbf{x}_{0n}$ , straightforwardly leading to

$$\frac{1}{V_{\mathbf{b}_n^d}} \int_{\mathbf{B}} \theta\left(\frac{1}{4}d^2 - |\mathbf{x} - \mathbf{x}_{0n}|^2\right) \varphi(\mathbf{x}) \, d\mathbf{x} \rightarrow \varphi(\mathbf{x}_{0n}) \quad \text{as } d \rightarrow 0,$$

which implies (6). □

**Corollary 1** *In the sense of distributions,*

$$\frac{1}{V_{\mathbf{B}_b^d}} \chi_{\mathbf{B}_b^d}(\mathbf{x}) \rightarrow \frac{1}{V_{\mathbf{B}}} \text{ as } d \rightarrow 0. \quad (7)$$

*Proof* According to the definition,

$$\frac{1}{V_{\mathbf{B}_b^d}} (\chi_{\mathbf{B}_b^d}, \varphi) = \frac{1}{V_{\mathbf{B}_b^d}} \int_{\mathbf{B}} \chi_{\mathbf{B}_b^d}(\mathbf{x}) \varphi(\mathbf{x}) \, d\mathbf{x} = \frac{1}{V_{\mathbf{B}_b^d}} \int_{\mathbf{B}_b^d} \varphi(\mathbf{x}) \, d\mathbf{x}.$$

As  $d \rightarrow 0$ ,  $V_{\mathbf{b}_n^d} \rightarrow V_{\mathbf{B}}$  for all  $n = 1, 2, \dots, N$ , and  $\mathbf{B}_b^d \rightarrow \mathbf{B}_b^0 = \mathbf{B} \setminus \mathbf{b}^0$ . Therefore,

$$\frac{1}{V_{\mathbf{B}_b^d}} \int_{\mathbf{B}_b^d} \varphi(\mathbf{x}) \, d\mathbf{x} \rightarrow \frac{1}{V_{\mathbf{B}}} \int_{\mathbf{B}_b^0} \varphi(\mathbf{x}) \, d\mathbf{x},$$

since  $\mathbf{b}^0$  is a finite set of isolated points which does not alter the value of the integral. This is equivalent to (7).  $\square$

Passing to the limit in (4) as  $d \rightarrow 0$  and making use of Lemma 1 and Corollary 1, it is straightforwardly derived that in the sense of distributions,

$$\rho^d \rightarrow \rho^0 \text{ as } d \rightarrow 0$$

where

$$\rho^0(\mathbf{x}) = \rho_{\text{bulk}}^0 + m_{\text{incl}} \sum_{n=1}^N \delta(\mathbf{x} - \mathbf{x}_{0n}), \quad (8)$$

with

$$\rho_{\text{bulk}}^0 = \frac{m_{\text{bulk}}}{V_{\mathbf{B}}}. \quad (9)$$

Apparently, (8) characterizes a continuum with  $N$  concentrated masses. Note that since  $\chi_{\mathbf{B}_b^0}$  is dimensionless and the spatial Dirac  $\delta$  has an SI unit of  $m^{-3}$ , so that both sides of (8) have the same SI units. It is noteworthy that (8) corresponds to the density of a continuum containing point inhomogeneities.

On the other hand, on the basis of Corollary 1 implying that, as  $d \rightarrow 0$ ,

$$\chi_{\mathbf{B}_b^d}(\mathbf{x}) = (1 - \phi_{\text{incl}}) \frac{V_{\mathbf{B}}}{V_{\mathbf{B}_b^d}} \chi_{\mathbf{B}_b^d}(\mathbf{x}) \rightarrow 1 - \phi_{\text{incl}}$$

in the sense of distributions, and on the basis of Lemma 1 which ensures that, as  $d \rightarrow 0$ ,

$$\chi_{\mathbf{b}_n^d}(\mathbf{x}) = \phi_{\text{incl}} V_{\mathbf{B}} \frac{1}{N V_{\mathbf{b}_n^d}} \chi_{\mathbf{b}_n^d}(\mathbf{x}) \rightarrow \phi_{\text{incl}} V_{\mathbf{B}} \cdot \frac{1}{N} \delta(\mathbf{x} - \mathbf{x}_{0n})$$

in the sense of distributions, for (5) it is derived that

$$E^d \rightarrow E^0 \text{ as } d \rightarrow 0,$$

in the sense of distributions, where

$$E^0(\mathbf{x}) = (1 - \phi_{\text{incl}}) E_{\text{bulk}} + \phi_{\text{incl}} V_{\mathbf{B}} E_{\text{incl}} \cdot \frac{1}{N} \sum_{n=1}^N \delta(\mathbf{x} - \mathbf{x}_{0n}), \quad \mathbf{x} \in \mathbf{B}. \quad (10)$$

Note that both sides of (10) also have the same SI units.

### 3 Reinforced isotropic linear elastic material

Let the material of  $\mathbf{B}$  be isotropic and linear elastic. Then, with the aid of the Lamé coefficients  $\lambda^d = \lambda^d(\mathbf{x})$  and  $\mu^d = \mu^d(\mathbf{x})$ , the constitutive equations for  $\mathbf{B}$  will have the following form:

$$\boldsymbol{\sigma}^d(\mathbf{x}) = \lambda^d(\mathbf{x}) \operatorname{tr} \boldsymbol{\varepsilon}^d(\mathbf{x}) \mathbb{I} + 2\mu^d(\mathbf{x}) \boldsymbol{\varepsilon}^d(\mathbf{x}), \quad \mathbf{x} \in \mathbf{B}. \quad (11)$$

Here  $\boldsymbol{\sigma}^d$  is the Cauchy stress tensor and  $\boldsymbol{\varepsilon}^d$  is the strain tensor of  $\mathbf{B}$ ,  $\operatorname{tr}$  is the trace operator,  $\mathbb{I}$  is the identity tensor.

*Remark 1* While the assumption that  $\mathbf{B}$  is isotropic is far from being natural, it is merely to simplify the governing system of partial differential equations. The more general assumption [25]

$$\boldsymbol{\sigma}^d(\mathbf{x}) = \mathbf{C}^d(\mathbf{x}) : \boldsymbol{\varepsilon}^d(\mathbf{x}), \quad (12)$$

could be accepted, where  $\mathbf{C}^d$  is the tensor of anisotropic coefficients, and the further analysis would be similar. For efficient ways of numerical implementation of  $\mathbf{C}^d$ , see also [26].

When  $\mathbf{B}$  is in equilibrium, the Cauchy stress satisfies the equilibrium equations

$$\nabla \cdot \boldsymbol{\sigma}^d(\mathbf{x}) + \rho^d(\mathbf{x}) \mathbf{F}(\mathbf{x}) = \mathbf{0}, \quad \mathbf{x} \in \mathbf{B}, \quad (13)$$

where  $\mathbf{F}$  is the density of body forces.

Limiting the consideration by linear kinematic assumptions, i.e.,

$$\boldsymbol{\varepsilon}^d(\mathbf{x}) = \frac{1}{2} \left[ \nabla \mathbf{u}^d(\mathbf{x}) + \left( \nabla \mathbf{u}^d(\mathbf{x}) \right)^T \right], \quad (14)$$

where  $\mathbf{u}^d$  is the microscopic displacement vector of  $\mathbf{B}$ , the superscript T denotes transposition, substituting (14) into (11) and the resulting stresses into (13), the Navier–Lamé equations are derived,

$$\nabla \cdot \left( \lambda^d(\mathbf{x}) \operatorname{tr} \left[ \nabla \mathbf{u}^d(\mathbf{x}) \right] \mathbb{I} + \mu^d(\mathbf{x}) \left[ \nabla \mathbf{u}^d(\mathbf{x}) + \left( \nabla \mathbf{u}^d(\mathbf{x}) \right)^T \right] \right) + \rho^d(\mathbf{x}) \mathbf{F}(\mathbf{x}) = \mathbf{0}, \quad \mathbf{x} \in \mathbf{B}. \quad (15)$$

For the sake of simplicity, assume that the Poisson's ratio of  $\mathbf{B}_b^d$  and  $\mathbf{b}_n^d$  are equal:  $\nu_1 = \nu_2 := \nu$ , so that

$$\lambda^d(\mathbf{x}) = \alpha E^d(\mathbf{x}), \quad \mu^d(\mathbf{x}) = \frac{1}{2} \beta E^d(\mathbf{x}), \quad \alpha = \frac{\nu}{(1+\nu)(1-2\nu)}, \quad \beta = \frac{1}{1+\nu},$$

where  $E^d$  is the Young's modulus of  $\mathbf{B}$ . This will reduce (15) to the following:

$$\nabla \cdot \left( E^d(\mathbf{x}) \left[ \alpha \operatorname{tr} \left[ \nabla \mathbf{u}^d(\mathbf{x}) \right] \mathbb{I} + \beta \left[ \nabla \mathbf{u}^d(\mathbf{x}) + \left( \nabla \mathbf{u}^d(\mathbf{x}) \right)^T \right] \right] \right) + \rho^d(\mathbf{x}) \mathbf{F}(\mathbf{x}) = \mathbf{0}, \quad \mathbf{x} \in \mathbf{B}. \quad (16)$$

The aim now is to show that

$$\mathbf{u}^d \rightarrow \mathbf{u}^0 \quad \text{as } d \rightarrow 0 \quad (17)$$

in the space of admissible displacements, where  $\mathbf{u}^0$  is the mesoscopic displacement of  $\mathbf{B}$  satisfying the Navier–Lamé equations

$$\nabla \cdot \left( E^0(\mathbf{x}) \left[ \alpha \operatorname{tr} \left[ \nabla \mathbf{u}^0(\mathbf{x}) \right] \mathbb{I} + \beta \left[ \nabla \mathbf{u}^0(\mathbf{x}) + \left( \nabla \mathbf{u}^0(\mathbf{x}) \right)^T \right] \right] \right) + \rho^0(\mathbf{x}) \mathbf{F}(\mathbf{x}) = \mathbf{0}, \quad \mathbf{x} \in \mathbf{B}. \quad (18)$$

Here,  $\rho^0$  and  $E^0$  are given by (8), (9), and (10), respectively.

### 3.1 The Bubnov–Galerkin procedure

In this section, it is shown that (17) holds, i.e., the general solution of (16) converges to the general solution of (18) as  $d \rightarrow 0$ . Various types of convergence between differential operators have been applied in diverse problems of elasticity theory and of mechanics in general [5]. The type of convergence mostly depends on the space where the corresponding coefficients of the operators converge. Specifically, if the coefficients converge in  $L^\infty$ , then the convergence of differential operators is referred to as  $G$ - (symmetric operators) or  $H$ -convergence (nonsymmetric operators) [3]. However, in this case,  $E^d \rightarrow E^0$  and  $\rho^d \rightarrow \rho_0$  as  $d \rightarrow 0$  in the sense of distributions. Therefore, the convergence between (16) and (18) is not referred to as  $H$ -convergence here.

In order to show that (17) holds, taking into account that the coefficients of (16) and (18) are distributions, their reduced basis solutions obtained by the Bubnov–Galerkin method [27] are used. For the sake of simplicity, (16) is written component-wise making use of Einstein's summation rule:

$$\frac{\partial}{\partial x_j} \left( E^d(\mathbf{x}) \left[ \alpha \frac{\partial u_i^d}{\partial x_l} \delta_l^j + \beta \left( \frac{\partial u_i^d}{\partial x_j} + \frac{\partial u_j^d}{\partial x_i} \right) \right] \right) + \rho^d(\mathbf{x}) F_i = 0, \quad i = 1, 2, 3. \quad (19)$$

Following to the standard steps of the Bubnov–Galerkin procedure, let  $\{\varphi_k(\mathbf{x})\}_{k=1}^K$  be a family of functions orthogonal in  $\Omega$  satisfying given boundary conditions on  $\partial\Omega$ , and seek the reduced basis solution of (19) as follows

$$u_i^d(\mathbf{x}) \approx \sum_{k=1}^K c_{ik}^d \varphi_k(\mathbf{x}) = \mathbf{c}_i^d \cdot \boldsymbol{\varphi}(\mathbf{x}). \quad (20)$$

Then, the Bubnov–Galerkin orthogonality conditions results in the following linear algebraic equations for the expansion coefficients  $c_i^d$  [27]:

$$\int_{\mathbf{B}} \frac{\partial}{\partial x_j} \left( E^d(\mathbf{x}) \left[ \alpha c_l^d \cdot \frac{\partial \boldsymbol{\varphi}}{\partial x_l} \delta_l^j + \beta \left( c_i^d \cdot \frac{\partial \boldsymbol{\varphi}}{\partial x_j} + c_j^d \cdot \frac{\partial \boldsymbol{\varphi}}{\partial x_i} \right) \right] \right) \varphi_{k'}(\mathbf{x}) \, d\mathbf{x} + f_{ik'}^d = 0, \quad k' = 1, \dots, K, \quad (21)$$

where

$$f_{ik'}^d = \int_{\mathbf{B}} \rho^d(\mathbf{x}) F_i(\mathbf{x}) \varphi_{k'}(\mathbf{x}) \, d\mathbf{x}.$$

Assuming that  $\mathbf{u}^d = 0$  on  $\partial\Omega$  which implies  $\boldsymbol{\varphi} = 0$  on  $\partial\Omega$  as well, and performing in (21) integration by parts, it is reduced to

$$\left[ E_{\text{bulk}} \int_{\mathbf{B}_b^d} + E_{\text{incl}} \sum_{n=1}^N \int_{\mathbf{b}_n^d} \right] \Phi_{ik'}(\mathbf{x}; \mathbf{c}_1^d, \mathbf{c}_2^d, \mathbf{c}_3^d) \, d\mathbf{x} - f_{ik'}^d = 0, \quad (22)$$

where

$$\Phi_{ik'}(\mathbf{x}; \mathbf{c}_1^d, \mathbf{c}_2^d, \mathbf{c}_3^d) = \left[ \alpha c_l^d \cdot \frac{\partial \boldsymbol{\varphi}}{\partial x_l} + \beta \left( c_i^d \cdot \frac{\partial \boldsymbol{\varphi}}{\partial x_j} + c_j^d \cdot \frac{\partial \boldsymbol{\varphi}}{\partial x_i} \right) \right] \frac{\partial \varphi_{k'}}{\partial x_j}.$$

Now let  $d \rightarrow 0$  and denote by  $\hat{\mathbf{c}}_i^0$  the limiting solution of (22). Then, in view of linearity of  $\Phi_{ik'}$  in  $\mathbf{c}_1^d$ ,  $\mathbf{c}_2^d$ , and  $\mathbf{c}_3^d$ , it is obtained that  $\hat{\mathbf{c}}_i^0$  satisfy

$$(1 - \phi_{\text{incl}}) E_{\text{bulk}} \int_{\mathbf{B}_b^0} \Phi_{ik'}(\mathbf{x}; \hat{\mathbf{c}}_1^0, \hat{\mathbf{c}}_2^0, \hat{\mathbf{c}}_3^0) \, d\mathbf{x} + \phi_{\text{incl}} \mathbf{V}_{\mathbf{B}} E_{\text{incl}} \cdot \frac{1}{N} \sum_{n=1}^N \Phi_{ik'}(\mathbf{x}_n^0; \hat{\mathbf{c}}_1^0, \hat{\mathbf{c}}_2^0, \hat{\mathbf{c}}_3^0) - f_{ik'}^0 = 0, \quad (23)$$

with

$$f_{ik'}^0 = \int_{\mathbf{B}} \rho^0(\mathbf{x}) F_i(\mathbf{x}) \varphi_{k'}(\mathbf{x}) \, d\mathbf{x}.$$

Denoting by  $c_i^0$  the expansion coefficients of the solution of (18), i.e.,

$$u_i^0(\mathbf{x}) \approx c_i^0 \cdot \boldsymbol{\varphi}(\mathbf{x}), \tag{24}$$

and substituting this approximate solution into (18), using the Bubnov–Galerkin orthogonality conditions and the definition of the Dirac distribution (1), the following system of linear algebraic equations is obtained for the expansion coefficients  $c_i^0$ :

$$(1 - \phi_{\text{incl}}) E_{\text{bulk}} \int_{\mathbf{B}_b^0} \Phi_{ik'}(\mathbf{x}; \mathbf{c}_1^0, \mathbf{c}_2^0, \mathbf{c}_3^0) d\mathbf{x} + \phi_{\text{incl}} V_{\mathbf{B}} E_{\text{incl}} \cdot \frac{1}{N} \sum_{n=1}^N \Phi_{ik'}(\mathbf{x}_n^0; \mathbf{c}_1^0, \mathbf{c}_2^0, \mathbf{c}_3^0) - f_{ik'}^0 = 0. \tag{25}$$

Evidently, (23) and (25) are the same systems meaning that  $\hat{c}_i^0 = c_i^0$ .

The well-known fact that, as  $K \rightarrow \infty$ , (20) and (24) converge to corresponding exact solutions in the space of admissible displacements [28], leads to the following assertion.

**Theorem 1** *In the space of admissible displacements, (17) holds for the general solutions of (16) with (4), (5) and of (18) with (8), (10).*

#### 4 Reinforced Mindlin–Reissner plate

Consider a particular case when  $\Omega = \{\mathbf{x} \in \mathbb{R}^3, 0 \leq x_1 \leq l_1, 0 \leq x_2 \leq l_2, -h \leq x_3 \leq h\}$  corresponding to the case when  $\mathbf{B}$  is a plate of constant thickness  $2h$ . Assume that  $d \ll h$ .

Accepting the Mindlin–Reissner assumptions, the microscopic displacement field of the plate is represented as [5]

$$\mathbf{u}^d(\mathbf{x}) = \left( u_1^d(x) - x_3 \phi_1^d(x), u_2^d(x) - x_3 \phi_2^d(x), u_3^d(x) \right)^T.$$

Here,  $u_1^d, u_2^d$  are the in-plane, and  $u_3^d$  is the out-of-plane displacements of the mid-surface  $x_3 = 0$ , denoted by  $\Omega_0$ ,  $\phi_1^d$  and  $\phi_2^d$  are the angles formed by the normal to the mid-surface with  $x_3$ .

The strain–displacement relations within Mindlin–Reissner theory are given according to (14),

$$\begin{aligned} \varepsilon_{ij}^d(\mathbf{x}) &= \frac{1}{2} \left[ \frac{\partial}{\partial x_j} \left( u_i^d(x) - x_3 \phi_i^d(x) \right) + \frac{\partial}{\partial x_i} \left( u_j^d(x) - x_3 \phi_j^d(x) \right) \right], \\ \varepsilon_{i3}^d(\mathbf{x}) &= \frac{\kappa}{2} \left[ \frac{\partial u_3^d}{\partial x_i} - \phi_i^d(x) \right], \quad i, j = 1, 2, \\ \varepsilon_{33}^d(\mathbf{x}) &\equiv 0. \end{aligned} \tag{26}$$

where  $\kappa = \text{const}$  is a (dimensionless) shear correction factor.

The stress–strain relation is given by the Hooke’s law

$$\begin{aligned} \begin{bmatrix} \sigma_{11}^d(\mathbf{x}) \\ \sigma_{22}^d(\mathbf{x}) \\ \sigma_{12}^d(\mathbf{x}) \\ \sigma_{13}^d(\mathbf{x}) \\ \sigma_{23}^d(\mathbf{x}) \end{bmatrix} &= \frac{E^d(\mathbf{x})}{1 - \nu^2} \begin{bmatrix} 1 & \nu & 0 & 0 & 0 \\ \nu & 1 & 0 & 0 & 0 \\ 0 & 0 & 1 - \nu & 0 & 0 \\ 0 & 0 & 0 & 1 - \nu & 0 \\ 0 & 0 & 0 & 0 & 1 - \nu \end{bmatrix} \begin{bmatrix} \varepsilon_{11}^d(\mathbf{x}) \\ \varepsilon_{22}^d(\mathbf{x}) \\ \varepsilon_{12}^d(\mathbf{x}) \\ \varepsilon_{13}^d(\mathbf{x}) \\ \varepsilon_{23}^d(\mathbf{x}) \end{bmatrix}, \\ \sigma_{33}^d(\mathbf{x}) &\equiv 0. \end{aligned}$$

The equilibrium equations are written for the stress, moment and shear resultants

$$N_{ij}^d(x) = \int_{-h}^h \sigma_{ij}^d(\mathbf{x}) dx_3, \quad M_{ij}^d(x) = \int_{-h}^h x_3 \sigma_{ij}^d(\mathbf{x}) dx_3, \quad Q_i^d(x) = \kappa \int_{-h}^h \sigma_{3i}^d(\mathbf{x}) dx_3, \quad i, j = 1, 2, \tag{27}$$



as follows (recall that the Einstein's summation rule is accepted):

$$\begin{aligned}\frac{\partial N_{ij}^d}{\partial x_j} &= 0, \\ \frac{\partial M_{ij}^d}{\partial x_j} - Q_i^d &= 0, \quad i = 1, 2, \\ \frac{\partial Q_j^d}{\partial x_j} + F &= 0.\end{aligned}$$

Here,  $F$  is an out-of-plane load applied to the plate. Substituting the above strain–displacement relations into the stress–strain relations, from the equilibrium equations, the following system of linear equations for  $u_i^d$  and  $\phi_j^d$  will be derived:

$$\begin{aligned}\frac{\partial}{\partial x_1} \left[ A_0^d(x) \left( \frac{\partial u_1^d}{\partial x_1} + \nu \frac{\partial u_2^d}{\partial x_2} \right) - A_1^d(x) \left( \frac{\partial \phi_1^d}{\partial x_1} + \nu \frac{\partial \phi_2^d}{\partial x_2} \right) \right] \\ + \frac{1-\nu}{2} \frac{\partial}{\partial x_2} \left[ A_0^d(x) \left( \frac{\partial u_1^d}{\partial x_2} + \frac{\partial u_2^d}{\partial x_1} \right) - A_1^d(x) \left( \frac{\partial \phi_1^d}{\partial x_2} + \frac{\partial \phi_2^d}{\partial x_1} \right) \right] &= 0, \\ \frac{1-\nu}{2} \frac{\partial}{\partial x_1} \left[ A_0^d(x) \left( \frac{\partial u_1^d}{\partial x_2} + \frac{\partial u_2^d}{\partial x_1} \right) - A_1^d(x) \left( \frac{\partial \phi_1^d}{\partial x_2} + \frac{\partial \phi_2^d}{\partial x_1} \right) \right] \\ + \frac{\partial}{\partial x_2} \left[ A_0^d(x) \left( \nu \frac{\partial u_1^d}{\partial x_1} + \frac{\partial u_2^d}{\partial x_2} \right) - A_1^d(x) \left( \nu \frac{\partial \phi_1^d}{\partial x_1} + \frac{\partial \phi_2^d}{\partial x_2} \right) \right] &= 0, \\ \frac{\partial}{\partial x_1} \left[ A_1^d(x) \left( \frac{\partial u_1^d}{\partial x_1} + \nu \frac{\partial u_2^d}{\partial x_2} \right) - A_2^d(x) \left( \frac{\partial \phi_1^d}{\partial x_1} + \nu \frac{\partial \phi_2^d}{\partial x_2} \right) \right] \\ + \frac{1-\nu}{2} \frac{\partial}{\partial x_2} \left[ A_1^d(x) \left( \frac{\partial u_1^d}{\partial x_2} + \frac{\partial u_2^d}{\partial x_1} \right) - A_2^d(x) \left( \frac{\partial \phi_1^d}{\partial x_2} + \frac{\partial \phi_2^d}{\partial x_1} \right) \right] &= 0, \\ &= \kappa \frac{1-\nu}{2} A_0^d(x) \left( \frac{\partial u_3^d}{\partial x_1} - \phi_1^d(x) \right), \\ \frac{1-\nu}{2} \frac{\partial}{\partial x_1} \left[ A_1^d(x) \left( \frac{\partial u_1^d}{\partial x_2} + \frac{\partial u_2^d}{\partial x_1} \right) - A_2^d(x) \left( \frac{\partial \phi_1^d}{\partial x_2} + \frac{\partial \phi_2^d}{\partial x_1} \right) \right] \\ + \frac{\partial}{\partial x_2} \left[ A_1^d(x) \left( \nu \frac{\partial u_1^d}{\partial x_1} + \frac{\partial u_2^d}{\partial x_2} \right) - A_2^d(x) \left( \nu \frac{\partial \phi_1^d}{\partial x_1} + \frac{\partial \phi_2^d}{\partial x_2} \right) \right] &= 0, \\ &= \kappa \frac{1-\nu}{2} A_0^d(x) \left( \frac{\partial u_3^d}{\partial x_2} - \phi_2^d(x) \right), \\ \frac{\partial}{\partial x_1} \left[ A_0^d(x) \left( \frac{\partial u_3^d}{\partial x_1} - \phi_1^d(x) \right) \right] + \frac{\partial}{\partial x_2} \left[ A_0^d(x) \left( \frac{\partial u_3^d}{\partial x_2} - \phi_2^d(x) \right) \right] &= -\frac{2}{\kappa(1-\nu)} F(x),\end{aligned}\tag{28}$$

where

$$A_p^d(x) = \int_{-h}^h \frac{E^d(\mathbf{x})}{1-\nu^2} x_3^p dx_3, \quad p = 0, 1, 2,$$

$A_1^d$  and  $A_2^d$  are the so-called extensional and bending stiffnesses.

Note that (28) is a system of five linear differential equations with respect to five unknown functions:  $u_i^d$ ,  $i = 1, 2, 3$ , and  $\phi_j^d$ ,  $j = 1, 2$ . Similar to Theorem 1 it is shown that as  $d \rightarrow 0$ ,

$$u_i^d \rightarrow u_i^0, \quad \phi_j^d \rightarrow \phi_j^0, \quad i = 1, 2, 3, \quad j = 1, 2,$$

where  $u_i^0$ ,  $i = 1, 2, 3$ , and  $\phi_j^0$ ,  $j = 1, 2$ , are determined from the corresponding system of differential equations with  $E^d (A_p^d)$  substituted by  $E^0$  (resp.  $A_p^0$ ).

Taking into account that for  $-h < x_{03n} < h$ ,  $n = 1, 2, \dots, N$ ,

$$\int_{-h}^h x_3^p \delta(\mathbf{x} - \mathbf{x}_{0n}) \, dx_3 = x_{03n}^p \delta(x - x_{0n}), \quad p = 0, 1, 2,$$

for the mesoscopic coefficients it is derived

$$A_p^0(x) = \begin{cases} \frac{1}{1-\nu^2} \left[ \frac{h^{p+1}}{p+1} (1 - \phi_{\text{incl}}) E_{\text{bulk}} + \phi_{\text{incl}} \mathbf{V} \mathbf{B} E_{\text{incl}} \cdot \frac{1}{N} \sum_{n=1}^N x_{03n}^p \delta(x - x_{0n}) \right], & p = 0, 2, \\ \frac{1}{1-\nu^2} \phi_{\text{incl}} \mathbf{V} \mathbf{B} E_{\text{incl}} \cdot \frac{1}{N} \sum_{n=1}^N x_{03n} \delta(x - x_{0n}), & p = 1. \end{cases} \quad (29)$$

#### 4.1 Numerical verification

In this section, the mesoscopic model of particle-reinforced Mindlin–Reissner plate is studied numerically. For the sake of simplicity, neglect the in-plane extension of the plate. Then, the moment and shear resultants are determined as follows:

$$\begin{aligned} M_{11}^d(x) &= -A_2^d(x) \left( \frac{\partial \phi_1^d}{\partial x_1} + \nu \frac{\partial \phi_2^d}{\partial x_2} \right), \quad M_{12}^d(x) = -\frac{1-\nu}{2} A_2^d(x) \left( \frac{\partial \phi_1^d}{\partial x_2} + \frac{\partial \phi_2^d}{\partial x_1} \right), \\ M_{22}^d(x) &= A_2^d(x) \left( \nu \frac{\partial \phi_1^d}{\partial x_1} + \frac{\partial \phi_2^d}{\partial x_2} \right), \\ Q_1^d(x) &= \kappa \frac{1-\nu}{2} A_0^d(x) \left( \frac{\partial u_3^d}{\partial x_1} - \phi_1^d(x) \right), \quad Q_2^d(x) = \kappa \frac{1-\nu}{2} A_0^d(x) \left( \frac{\partial u_3^d}{\partial x_2} - \phi_2^d(x) \right). \end{aligned} \quad (30)$$

Equilibrium equations (28) take the following form:

$$\begin{aligned} \frac{\partial}{\partial x_1} \left[ A_2^d(x) \left( \frac{\partial \phi_1^d}{\partial x_1} + \nu \frac{\partial \phi_2^d}{\partial x_2} \right) \right] + \frac{1-\nu}{2} \frac{\partial}{\partial x_2} \left[ A_2^d(x) \left( \frac{\partial \phi_1^d}{\partial x_2} + \frac{\partial \phi_2^d}{\partial x_1} \right) \right] \\ + \kappa \frac{1-\nu}{2} A_0^d(x) \left( \frac{\partial u_3^d}{\partial x_1} - \phi_1^d(x) \right) &= 0, \\ \frac{1-\nu}{2} \frac{\partial}{\partial x_1} \left[ A_2^d(x) \left( \frac{\partial \phi_1^d}{\partial x_2} + \frac{\partial \phi_2^d}{\partial x_1} \right) \right] + \frac{\partial}{\partial x_2} \left[ A_2^d(x) \left( \nu \frac{\partial \phi_1^d}{\partial x_1} + \frac{\partial \phi_2^d}{\partial x_2} \right) \right] \\ + \kappa \frac{1-\nu}{2} A_0^d(x) \left( \frac{\partial u_3^d}{\partial x_2} - \phi_2^d(x) \right) &= 0, \\ \frac{\partial}{\partial x_1} \left[ A_0^d(x) \left( \frac{\partial u_3^d}{\partial x_1} - \phi_1^d(x) \right) \right] + \frac{\partial}{\partial x_2} \left[ A_0^d(x) \left( \frac{\partial u_3^d}{\partial x_2} - \phi_2^d(x) \right) \right] + \frac{2}{\kappa(1-\nu)} F(x) &= 0. \end{aligned} \quad (31)$$

Let the plate be clamped at the boundary implying

$$u_3^d = \phi_1^d = \phi_2^d = 0, \quad x \in \partial\Omega_0.$$

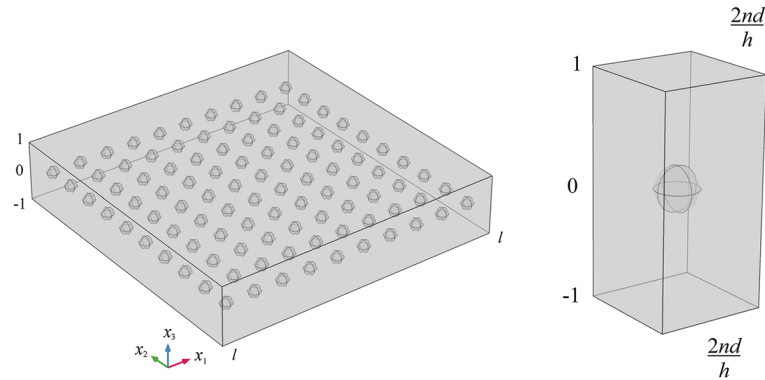


**Fig. 2** A thick Mindlin–Reissner plate with  $N = 100$  spherical inclusions

Also let  $l_1 = l_2 = l$  and rescale  $\mathbf{x}$  by  $h$ ,  $E^d$  by  $E_{\text{bulk}}$ ,  $A_k^d$  by  $h^{k+1} E_{\text{bulk}}$ ,  $k = 0, 2$ , and  $F$  by  $E_{\text{bulk}}$ . Since as a result of rescaling, system (31) refrains its form, new functions and variables are not introduced. Then, the general solution of (31) can be represented as follows:

$$u_3^d(x) = \sum_{k=1}^K c_{u_3k}^d \varphi_k(x), \quad \phi_1^d(x) = \sum_{k=1}^K c_{\phi_1k}^d \varphi_k(x), \quad \phi_2^d(x) = \sum_{k=1}^K c_{\phi_2k}^d \varphi_k(x), \quad (32)$$

with

$$\varphi_k(x) = \sin(\lambda_k x_1) \sin(\lambda_k x_2), \quad \lambda_k = \frac{\pi k}{l_h}, \quad l_h = \frac{l}{h}.$$

Using the Bubnov–Galerkin procedure, the following system of linear algebraic equations for  $c_{u_3k}^d$ ,  $c_{\phi_1k}^d$ , and  $c_{\phi_2k}^d$  is eventually derived:

$$\begin{bmatrix} \mathbf{B}^{u_3,d} & \mathbf{B}^{\phi_1,d} & \mathbf{B}^{\phi_2,d} \\ \mathbf{C}^{u_3,d} & \mathbf{C}^{\phi_1,d} & \mathbf{C}^{\phi_2,d} \\ \mathbf{D}^{u_3,d} & \mathbf{D}^{\phi_1,d} & \mathbf{D}^{\phi_2,d} \end{bmatrix} \begin{bmatrix} \mathbf{c}_{u_3}^d \\ \mathbf{c}_{\phi_1}^d \\ \mathbf{c}_{\phi_2}^d \end{bmatrix} = \begin{bmatrix} \mathbf{0} \\ \mathbf{0} \\ \mathbf{F} \end{bmatrix}, \quad (33)$$

where

$$\begin{aligned} B_{k,k'}^{u_3,d} &= \kappa \frac{1-\nu}{2} \int_0^{l_h} \int_0^{l_h} A_0^d(x) \frac{\partial \varphi_k}{\partial x_1} \varphi_{k'}(x) \, dx, \\ B_{k,k'}^{\phi_1,d} &= - \int_0^{l_h} \int_0^{l_h} \left[ A_2^d(x) \left( \frac{\partial \varphi_k}{\partial x_1} \frac{\partial \varphi_{k'}}{\partial x_1} + \frac{1-\nu}{2} \frac{\partial \varphi_k}{\partial x_2} \frac{\partial \varphi_{k'}}{\partial x_2} \right) + \kappa \frac{1-\nu}{2} A_0^d(x) \varphi_k(x) \varphi_{k'}(x) \right] dx, \\ B_{k,k'}^{\phi_2,d} &= - \int_0^{l_h} \int_0^{l_h} A_2^d(x) \left( \nu \frac{\partial \varphi_k}{\partial x_2} \frac{\partial \varphi_{k'}}{\partial x_1} + \frac{1-\nu}{2} \frac{\partial \varphi_k}{\partial x_1} \frac{\partial \varphi_{k'}}{\partial x_2} \right) dx, \\ C_{k,k'}^{u_3,d} &= \kappa \frac{1-\nu}{2} \int_0^{l_h} \int_0^{l_h} A_0^d(x) \frac{\partial \varphi_k}{\partial x_2} \varphi_{k'}(x) \, dx, \\ C_{k,k'}^{\phi_1,d} &= - \int_0^{l_h} \int_0^{l_h} A_2^d(x) \left( \nu \frac{\partial \varphi_k}{\partial x_1} \frac{\partial \varphi_{k'}}{\partial x_2} + \frac{1-\nu}{2} \frac{\partial \varphi_k}{\partial x_2} \frac{\partial \varphi_{k'}}{\partial x_1} \right) dx, \\ C_{k,k'}^{\phi_2,d} &= - \int_0^{l_h} \int_0^{l_h} \left[ A_2^d(x) \left( \frac{1-\nu}{2} \frac{\partial \varphi_k}{\partial x_1} \frac{\partial \varphi_{k'}}{\partial x_1} + \frac{\partial \varphi_k}{\partial x_2} \frac{\partial \varphi_{k'}}{\partial x_2} \right) + \kappa \frac{1-\nu}{2} A_0^d(x) \varphi_k(x) \varphi_{k'}(x) \right] dx, \\ D_{k,k'}^{u_3,d} &= \int_0^{l_h} \int_0^{l_h} A_0^d(x) \left( \frac{\partial \varphi_k}{\partial x_1} \frac{\partial \varphi_{k'}}{\partial x_1} + \frac{\partial \varphi_k}{\partial x_2} \frac{\partial \varphi_{k'}}{\partial x_2} \right) dx, \\ D_{k,k'}^{\phi_1,d} &= \int_0^{l_h} \int_0^{l_h} A_0^d(x) \varphi_k(x) \frac{\partial \varphi_{k'}}{\partial x_1} dx, \end{aligned}$$

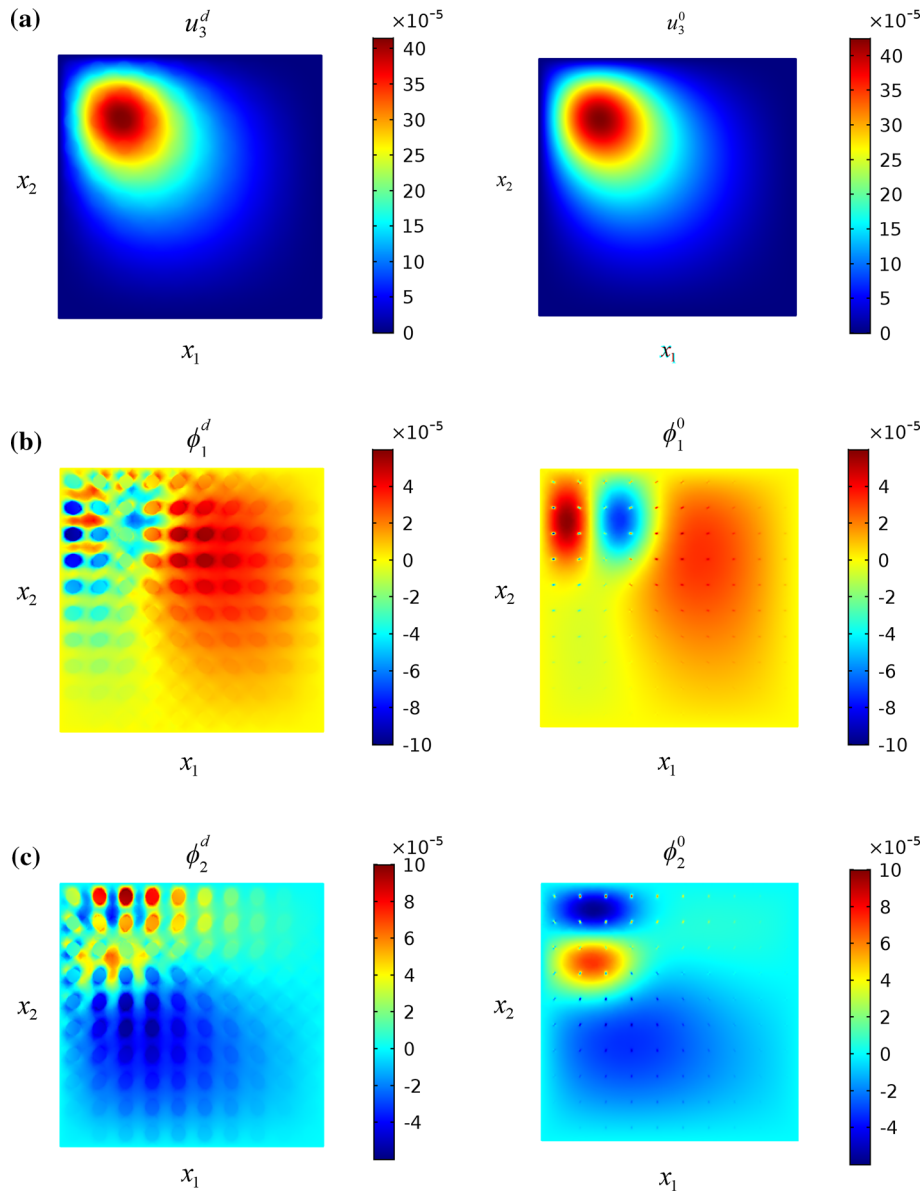


**Fig. 3** Generalized displacements of the plate mid-plane: **a**  $u_3^d$ ,  $d/h = 0.25$  (left) and  $u_3^0$  (right); **b**  $\phi_1^d$ ,  $d/h = 0.25$  (left),  $\phi_1^0$  (right) **c**  $\phi_2^d$ ,  $d/h = 0.25$  (left),  $\phi_2^0$  (right)

$$D_{k,k'}^{\phi_2,d} = \int_0^{l_h} \int_0^{l_h} A_0^d(x) \varphi_k(x) \frac{\partial \varphi_{k'}}{\partial x_2} dx,$$

$$F_{k'} = -\frac{2}{\kappa(1-\nu)} \int_0^{l_h} \int_0^{l_h} F(x) \varphi_{k'}(x) dx.$$

Due to linearity of (33), the mesoscopic model for a particle-reinforced Mindlin–Reissner plate is described by its limit as  $d \rightarrow 0$ , i.e., by (31) with  $A_k^d$  substituted by  $A_k^0$  (29),  $k = 0, 2$ .

For computations let  $l_h = 5$ ,  $N = 100$ ,  $K = 100$ ,  $\nu = 0.3$ ,  $\kappa = 5/6$ ,  $E_{incl}/E_{bulk} = 3$ ,  $F(x) = 10^{-3} \chi_{[0.5,1.5] \times [3.5,4.5]}(x)$ . Let  $x_{01n} = x_{02n} = 2nd/h$ ,  $x_{03n} \equiv 0.5$ ,  $n = 1, 2, \dots, 10$ , i.e., the inclusions are distributed uniformly over the plate mid-plane  $\Omega_0$  (see Fig. 2).

The main aim of this section is to numerically show that as  $d \rightarrow 0$ , generalized displacements and quantities (30) converge to corresponding quantities with superscript 0. To this aim, prescribe positive values to  $d/h$  and compare the corresponding quantities with the case when  $d \rightarrow 0$  (mesoscopic model). The components of the

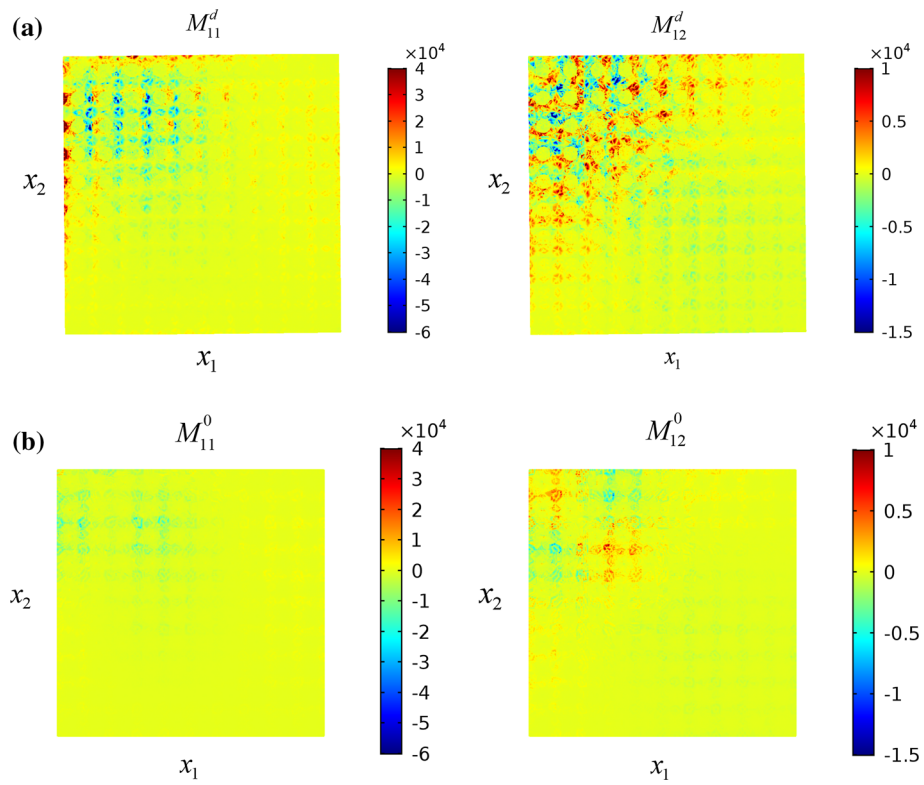


Fig. 4 Moment resultants: **a**  $d/h = 0.25$ ; **b**  $d \rightarrow 0$

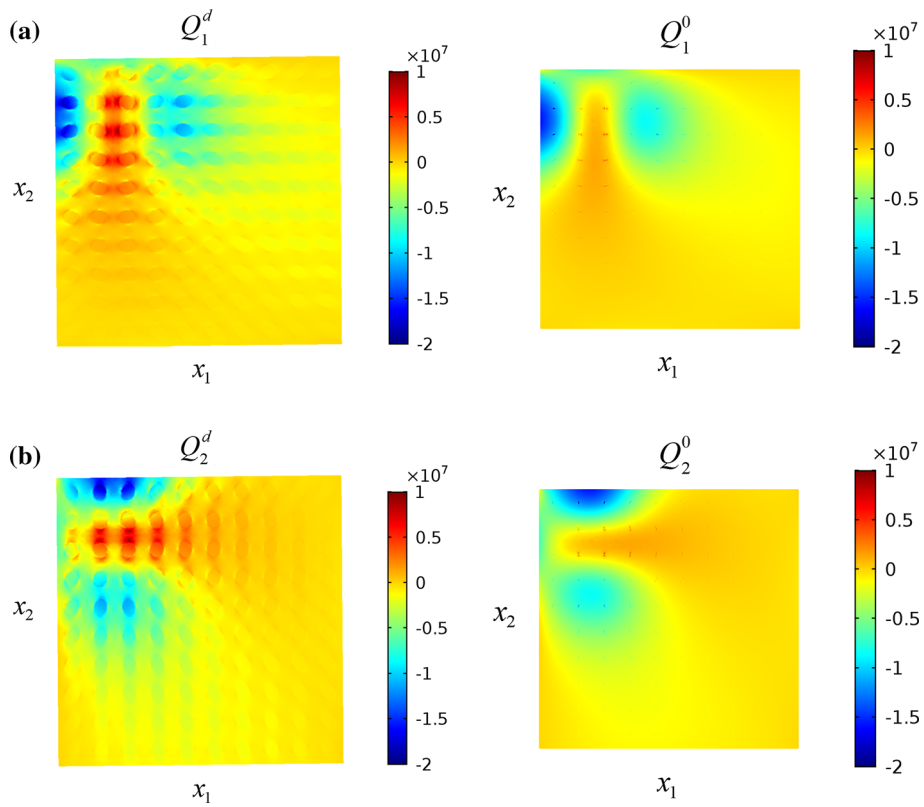


Fig. 5 Shear resultants: **a**  $Q_1^d$ ,  $d/h = 0.25$  (left),  $Q_1^0$  (right); **b**  $Q_2^d$ ,  $d/h = 0.25$  (left),  $Q_2^0$  (right)

**Table 1** Maximal absolute values of plate mid-plane vertical displacements, moment and shear resultants for different values of  $d/h$ 

$d/h$	$\max_{x \in \Omega_0}  u_3^d $	$\max_{x \in \Omega_0}  \phi_1^d $	$\max_{x \in \Omega_0}  \phi_2^d $	$\max_{x \in \Omega_0}  M_{11}^d $	$\max_{x \in \Omega_0}  M_{12}^d $	$\max_{x \in \Omega_0}  M_{22}^d $	$\max_{x \in \Omega_0}  Q_1^d $	$\max_{x \in \Omega_0}  Q_2^d $
1/4	$4.15 \times 10^{-4}$	$1.05 \times 10^{-4}$	$1.05 \times 10^{-4}$	$1.87 \times 10^5$	$4.98 \times 10^4$	$2.43 \times 10^5$	$1.74 \times 10^7$	$1.9 \times 10^7$
1/8	$4.23 \times 10^{-4}$	$1.12 \times 10^{-4}$	$1.06 \times 10^{-4}$	$1.25 \times 10^5$	$3.6 \times 10^4$	$2.04 \times 10^5$	$1.77 \times 10^7$	$1.94 \times 10^7$
1/16	$4.24 \times 10^{-4}$	$1.13 \times 10^{-4}$	$1.06 \times 10^{-4}$	$7.14 \times 10^4$	$2.48 \times 10^4$	$7.95 \times 10^4$	$1.8 \times 10^7$	$2 \times 10^7$
$\rightarrow 0$	$4.25 \times 10^{-4}$	$1.14 \times 10^{-4}$	$1.06 \times 10^{-4}$	$3.7 \times 10^4$	$1.39 \times 10^4$	$3.96 \times 10^4$	$1.84 \times 10^7$	$2.07 \times 10^7$

generalized displacement, the moment resultants and shear resultants of the plate mid-plane  $\Omega_0$  are plotted in Figs. 3, 4 and 5. Based on the results of plots and numerical evaluation of the representative quantities (30), presented in Table 1, it becomes evident that as  $d/h \rightarrow 0$ ,  $u_3^d \nearrow u_3^0$ ,  $\phi_i^d \nearrow \phi_i^0$ ,  $M_{ij}^d \searrow M_{ij}^0$ , and  $Q_i^d \nearrow Q_i^0$ ,  $i, j = 1, 2$ .

## 5 Conclusions and future work

Multiscale modeling of composites is one of the most efficient ways of accurate measuring of the effect that different types of microstructural peculiarities have on the macroscopic performance of the composite. This is equally important for evaluating the efficiency of practical use of composites with given microstructure and for estimating the opportunities of specific microstructural design of composites promising an improved performance for them at the macroscale. Being a powerful tool for deriving the material parameters of reinforced composites at the macroscale for a given microstructure, homogenization not always allows to include all the microscopic features into the final expressions for the effective or homogenized parameters explicitly. An example of such a feature is the location of individual particles in the case of particle-reinforced composites.

This study is an attempt to fill this gap by suggesting a model for particle-reinforced composites allowing to express their material properties in terms of all features of individual particles, such as Young's modulus and spatial location. Starting from the microscopic model where the composite is represented as a continuum reinforced with identical spherical inclusions and letting the diameter of the inclusions decrease to 0, the mesoscopic model is derived where particles are represented as point inhomogeneities characterized by Dirac distribution concentrated at the centers of the inclusions.

Future developments toward extension of the model derived in this paper are designed in the following directions:

1. Instead of unnatural assumption about isotropic structure of  $\mathbf{B}$ , a general anisotropy given by (12) will be considered.
2. While the geometrically nonlinear case with  $\boldsymbol{\varepsilon}^d(\mathbf{x}) = \frac{1}{2} \left[ \nabla \mathbf{u}^d(\mathbf{x}) + \left( \nabla \mathbf{u}^d(\mathbf{x}) \right)^T \right]$  used instead of (14), seems to be quite similar to the case considered in this paper due to linearity of Navier–Lamé equations with respect to  $E^d$  and  $\rho^d$ , the case of physical nonlinearity, i.e., when the constitutive law is nonlinear in  $\lambda^d$  and  $\mu^d$ , unlike (11), remains quite challenging. This is, first of all, conditioned by the fact that the material parameters in the mesoscopic model are, in general, distributions, and the theory of nonlinear distributions must be involved for a proper model analysis.
3. Relax the strict assumptions on the bulk and particles, e.g., incorporate the interface defects model developed in [23] into the current mesoscopic model, allow inclusions to interact with each other during deformation [24], etc.
4. Motivated by studies similar to [29] in which a nonpiezoelectric matrix is reinforced by piezoelectric particles to make the composite reacting to external electrical fields, the case of multi-phase particles will also be a part of future work.

**Acknowledgements** Prof. Min Tang (Institute of Natural Sciences, Shanghai Jiao Tong University, China) described the idea of mesoscale modeling during one of our insightful discussions. Dr. Hayk Aleksanyan (Institute of Mathematics, NAS of Armenia) helped to clarify some aspects of distributional limit. Dr. Shant Arakelyan (Yerevan State University) helped me to carry out the simulations. Extended discussions with Prof. Marcin Kamiński (Lodz University, Poland) and Prof. Lei Zhang (Institute of Natural Sciences, Shanghai Jiao Tong University, China), as well as the unbiased criticism of three referees substantially contributed to the revised version of the manuscript. I heartily acknowledge all of them. The support of the State Administration of Foreign Expert Affairs of China is acknowledged.

## References

1. Panasenko, G.: *Multi-scale Modelling for Structures and Composites*. Springer, Berlin (2005)
2. Steinhäuser, M.O.: *Computational Multiscale Modeling of Fluids and Solids: Theory and Applications*, 2nd edn. Springer, Berlin (2017)
3. Tartar, L.: *The General Theory of Homogenization. A Personalized Introduction*. Springer, Heidelberg (2009)
4. Bakhvalov, N., Panasenko, G.: *Homogenization: Averaging Processes in Periodic Media*. Kluwer, Dordrecht (1989)
5. Lewiński, T., Telega, J.J.: *Plates, Laminates and Shells: Asymptotic Analysis and Homogenization*. World Scientific Publishing, Singapore (2000)
6. Torquato, S.: *Random Heterogeneous Materials: Microstructure and Macroscopic Properties*. Springer, New York (2002)
7. Milton, G.W.: *The Theory of Composites*. Cambridge University Press, Cambridge (2004)
8. Vaezi, M., Seitz, H., Yang, S.: A review on 3D micro-additive manufacturing technologies. *Int. J. Adv. Manuf. Technol.* **67**(5–8), 1721–1754 (2013)
9. Wriggers, P., Hain, M.: Micro-meso-macro modelling of composite materials. In: Oñate, E., Owen, R. (eds.) *Computational Plasticity*. Springer, Berlin (2007)
10. Dvorak, G.J.: *Micromechanics of Composite Materials*. Springer, Dordrecht (2013)
11. Kushnnevsky, V., Morachkovsky, O., Altenbach, H.: Identification of effective properties of particle reinforced composite materials. *Comput. Mech.* **22**(4), 317–325 (1998)
12. Altenbach, H.: Modelling of anisotropic behavior in fiber and particle reinforced composites. In: Sadowski, T. (ed.) *Multiscale Modelling of Damage and Fracture Processes in Composite Materials*. CISM International Centre for Mechanical Sciences (Courses and Lectures), vol. 474. Springer, Vienna (2005)
13. Picu, C.R., Sorohan, S., Soare, M.A., Constantinescu, D.M.: Designing particulate composites: the effect of variability of filler properties and filler spatial distribution. In: Trovalusci, P. (ed.) *Materials with Internal Structure Multiscale and Multifield Modeling and Simulation*, pp. 89–108. Springer, Berlin (2016)
14. Schindler, S., Mergheim, J., Zimmermann, M., Aurich, J.C., Steinmann, P.: Numerical homogenization of elastic and thermal material properties for metal matrix composites (MMC). *Contin. Mech. Thermodyn.* **29**(1), 51–75 (2017)
15. Gallican, V., Brenner, R.: Homogenization estimates for the effective response of fractional viscoelastic particulate composites. *Contin. Mech. Thermodyn.* (2018). <https://doi.org/10.1007/s00161-018-0741-8>
16. Kamiński, M.: Deterministic and probabilistic homogenization limits for particle-reinforced composites with nearly incompressible components. *Compos. Struct.* **187**, 36–47 (2018)
17. Muc, A., Barski, M.: Design of particulate-reinforced composite materials. *Materials* **11**, 234 (2018)
18. German, R.M.: *Particulate Composites: Fundamentals and Applications*. Springer, Cham (2016)
19. Altenbach, H., Altenbach, J., Kissing, W.: *Mechanics of Composite Structural Elements*, 2nd edn. Springer, Singapore (2018)
20. Nazarenko, L., Bargmann, S., Stolarski, H.: Closed-form formulas for the effective properties of random particulate nanocomposites with complete Gurtin–Murdoch model of material surfaces. *Contin. Mech. Thermodyn.* **29**(1), 77–96 (2017)
21. Nazarenko, L., Stolarski, H., Altenbach, H.: Effective properties of particulate composites with surface-varying interphases. *Compos. Part B* **149**, 268–284 (2018)
22. Kamiński, M.: Homogenization of particulate and fibrous composites with some non-Gaussian material uncertainties. *Compos. Struct.* **210**, 778–786 (2019)
23. Sokolovski, D., Kamiński, M.: Homogenization of carbon/polymer composites with anisotropic distribution of particles and stochastic interface defects. *Acta Mech.* **229**, 3727–3765 (2018)
24. Ju, J.W., Yanase, K.: Micromechanics and effective elastic moduli of particle-reinforced composites with near-field particle interactions. *Acta Mech.* **215**, 135–153 (2010)
25. Ambarcumyan, S.A.: *Theory of Anisotropic Plates: Strength, Stability, and Vibrations*. Hemisphere Publishing, Washington (1991)
26. Nordmann, J., Abmus, M., Altenbach, H.: Visualising elastic anisotropy—theoretical background and computational implementation. *Contin. Mech. Thermodyn.* **30**(4), 689–708 (2018)
27. Quarteroni, A., Manzoni, A., Negri, F.: *Reduced Basis Methods for Partial Differential Equations*. Springer, Cham (2016)
28. Mikhlin, S.G.: *Error Analysis in Numerical Processes*. Wiley, Chichester (1991)
29. Lin, C.-H., Muliana, A.: Micromechanics models for the effective nonlinear electro-mechanical responses of piezoelectric composites. *Acta Mech.* **224**(7), 1471–1492 (2013)